Late stages of the Zika virus life cycle are impaired by a selective TRPML2 agonist

Kerstin K. Schwickert[1,2,3], Mirco Glitscher[2], Daniela Bender[2], Robin Murra[2], Kevin Schwickert[4], Steffen Pfalzgraf[2], Tanja Schirmeister[4], Ute A. Hellmich[1,5,6,*,**], Eberhard Hildt[2,*,**]

[1]Faculty of Chemistry and Earth Sciences, Institute of Organic Chemistry and Macromolecular Chemistry, Friedrich Schiller University, Jena, Germany

[2]Department of Virology, Paul-Ehrlich-Institut, 63225 Langen, Germany

[3]Department of Chemistry, Johannes Gutenberg-University, 55122 Mainz, Germany

[4]Institute of Pharmaceutical and Biomedical Sciences, Johannes Gutenberg-University, 55122 Mainz, Germany

[5]Centre for Biomolecular Magnetic Resonance (BMRZ), Goethe University, Frankfurt, Germany

[6]Cluster of Excellence "Balance of the Microverse", Friedrich Schiller University, Jena, Germany

*to whom correspondence should be addressed: eberhard.hildt@pei.de or ute.hellmich@uni-jena.de

**shared senior authorship

Abstract

The flavivirus genus includes human pathogenic viruses such as Dengue (DENV), West Nile (WNV) and Zika virus (ZIKV) posing a global health threat due to limited treatment options. Ion channels are crucial for various viral life cycle stages, but their potential as targets for antivirals is often not fully realized due to the lack of selective modulators. Here, we observe that the human endolysosomal cation channel TRPML2 agonist ML2-SA1 impairs the late life cycle stages of ZIKV, thus underscoring TRPML2 as a promising antiviral target. Upon treatment with ML2-SA1, levels of intracellular genomes and number of released virus particles of two different ZIKV isolates were significantly reduced. ML2-SA1-treated cells displayed enlarged vesicular structures and multivesicular bodies with ZIKV envelope protein accumulation. However, no increased ZIKV degradation in lysosomal compartments was observed. Rather, the antiviral effect of ML2-SA1 seemed to manifest by the compound's negative impact on genome replication. Moreover, ML2-SA1 treatment also led to intracellular cholesterol accumulation. ZIKV as well as many other viruses including the Orthohepevirus Hepatitis E virus (HEV) rely on the endolysosomal system and are affected by intracellular cholesterol levels to complete their life cycle. Since we observed ML2-SA1 to also negatively impact HEV infections in vitro, this compound may harbor a broader antiviral potential through perturbing the intracellular cholesterol distribution. Besides underscoring the potential of TRPML2 as a promising target for combatting viral infections, we uncover a tentative connection between this protein and cholesterol distribution within the context of infectious diseases.

Keywords: TRP channel, TRPML, Zika virus, flavivirus, Hepatitis E virus, cholesterol

1 Introduction

Zika virus (ZIKV) is a member of the *Flaviviridae* family and gained public attention during a major outbreak in the Americas in 2015/2016 when the infection was first associated with severe neurological complications, such as neonatal microcephaly (Schuler-Faccini et al., 2016). Until now, no specific treatment or prophylactic vaccine is available. ZIKV uses clathrin-mediated endocytosis to enter host cells (Agrelli et al., 2019). It is assumed that subsequent exposure to the acidic environment of the endolysosomal system triggers conformational changes of the ZIKV envelope (E) glycoprotein, which leads to membrane fusion and release of the viral RNA (Dai et al., 2016; Nour et al., 2013)**.** Due to their involvement in viral trafficking and release, endolysosomal ion channels have garnered increasing attention in infectious diseases and as potential antiviral targets (Chao et al., 2023; Grimm et al., 2017; Spix et al., 2020).

The three members of the human transient receptor potential mucolipin (TRPML) subfamily of ion channels mediate the pH-dependent cation release from the endolysosomal system and are involved in membrane trafficking and autophagy (Goretzki et al., 2021; Kim et al., 2009; Li et al., 2017; Sun et al., 2000; Vergarajauregui et al., 2008; Viet et al., 2019; Zeevi et al., 2009). TRPML2 is mainly expressed in lymphocytes and other cells of the immune system (García-Añoveros and Wiwatpanit, 2014). The expression of TRPML2 in mouse macrophages is strongly upregulated after Toll-like receptor activation and TRPML2 plays a role in chemokine and cytokine secretion of macrophages (Plesch et al., 2018; Sun et al., 2015). TRPML2 was reported as a putative interferon-stimulated gene and a potential function of TRPML2 in the innate immune response and during viral infections has been suggested (Lanford et al., 2006; Rinkenberger and Schoggins, 2018; Schoggins, 2019; Spix et al., 2020). Overexpression of TRPML2 in A549 cells was shown to increase infection with endocytosed RNA virus families including *Flaviviridae* (e.g. ZIKV) and *Orthomyxoviridae* (e.g. Influenza A virus (IAV)) by enhancing viral trafficking efficiency through the endolysosomal system (Rinkenberger and Schoggins, 2018). A knockout of TRPML2 decreased infection with IAV (Rinkenberger and Schoggins, 2018). Together, these data indicate that TRPML2 may be a promising antiviral target.

Several synthetic TRPML agonists are available (Chen et al., 2014; Grimm et al., 2012, 2010; Plesch et al., 2018; Shen et al., 2012). Their application to cells increases channel-mediated Ca^{2+} flux from endosomes and lysosomes into the cytosol, thereby influencing vesicular fusion and fission, vesicular trafficking, lysosomal exocytosis and autophagy (Medina et al., 2015; Samie et al., 2013). Treatment with the unselective TRPML channel agonist ML-SA1 (Shen et al., 2012) reduced DENV2 and ZIKV mRNA, protein and the amount of released infectious particles in a dose-dependent manner in A549 and Huh7 cells (Xia et al., 2020). The authors suggested that viral entry, but not the later stages of the DENV2 and ZIKV life cycles were affected by ML-SA1 (Xia et al., 2020). In contrast, a shared TRPML1 and TRPML3 agonist, MK6-83 (Chen et al., 2014), did not display antiviral potential, while the selective TRPML3 agonist SN-2 (Grimm et al., 2010) provoked an antiviral effect (Xia et al., 2020). It was postulated that the antiviral activity of ML-SA1 and SN-2 may be related to effects on TRPML2 and TRPML3 channel activity and expression levels (Xia et al., 2021). However, to date it remains unclear which of the three human TRPML channels are important for different stages during viral infection, and whether all three proteins are equally suited as antiviral targets.

For TRPML2, a potent selective agonist, ML2-SA1 is available (Plesch et al., 2018) that allowed us to investigate the specific role of TRPML2 for flaviviral infections *in vitro*. Two ZIKV isolates, a representative of the Asian

lineage (ZIKV French Polynesia) and a representative of the African lineage (ZIKV Uganda), were used. We found that independent of the viral lineage, ML2-SA1 treatment impaired the late stages of the ZIKV life cycle. This suggests a role for TRPML2 in flaviviral replication. We also observed a redistribution of intracellular cholesterol in ML2-SA1-treated cells. Notably, cholesterol-accumulation controls the release pathway of Hepatitis E virus (HEV) negatively, resulting in a lysosomal degradation of capsid structures (Glitscher et al., 2021b) explaining the antiviral effect of ML2-SA1 that we observed against this virus. All in all, this undermines the suitability of TRPML2 as a target for antivirals against ZIKV as well as HEV, and the selective endolysosomal channel agonist ML2-SA1 as a promising lead for novel antiviral compounds.

2 Materials & Methods

2.1 Cells and viruses

Human epithelial lung carcinoma cells (A549, ATCC CCL-185) and African green monkey kidney (Vero, ATCC CCL-81) cells were maintained in Dulbecco's modified Eagle medium (DMEM) containing 4.5 g/L D-glucose (Sigma Aldrich, Bio&Sell) supplemented with 10% fetal bovine serum (FBS, Bio&Sell), 100 U/mL penicillin and 100 µg/mL streptomycin (Paul-Ehrlich-Institute central laboratory) in 5% CO_2 and 95% relative humidity at 37 °C. For ZIKV infection experiments, cells were infected with either the ZIKV French Polynesia (H/PF/2013) or the Uganda (976 Uganda) isolate (both purchased from the European Virus Archive) with a multiplicity of infection (MOI) of 1. Unless otherwise stated, the inoculum was removed 16 h post infection and cells were washed once with PBS (phosphate buffered saline). At the desired time points, supernatants were collected and stored at -80 °C (where applicable) and cells were washed with PBS and lysed for subsequent experiments. Treatment with compounds was started two hours before infection and substances were refreshed during infection and 16 h and 24 h post infection to guarantee constant levels of compounds in cells. For HEV infection experiments, persistently HEV-infected A549 cells (parental A549 cells initially infected with HEV genotype 3c isolate 47832c (Johne et al., 2014)) were used and cells were treated with ML2-SA1 for 24 h.

2.2 TRPML agonists and other compounds

The non-specific TRPML agonist ML-SA1 was purchased from Merck KGaA. The selective TRPML2 agonist ML2-SA1 was synthesized according to a two-step procedure from McIntosh *et al*. (McIntosh et al., 2012) and Plesch *et al*. (Plesch et al., 2018). Starting from 2,6-dichlorobenzaldehyde, the benzaldoxime ***(2)*** was prepared by treatment with hydroxylamine hydrochloride. In the second step, the benzaldoxime ***(2)*** was brought to reaction with norbornene in the presence of (bis(trifluoroacetoxy)iodo)benzene (PIFA) to yield ML2-SA1 as a mixture of two enantiomers (for details see SI and Fig. S1–S4). Bafilomycin A1 was purchased from Sigma-Aldrich, Ribavirin from Selleckchem and Leupeptin from AppliChem GmbH. All compound stocks for biological assays were prepared in dimethyl sulfoxide (DMSO) except for Leupeptin, which was dissolved in H_2O.

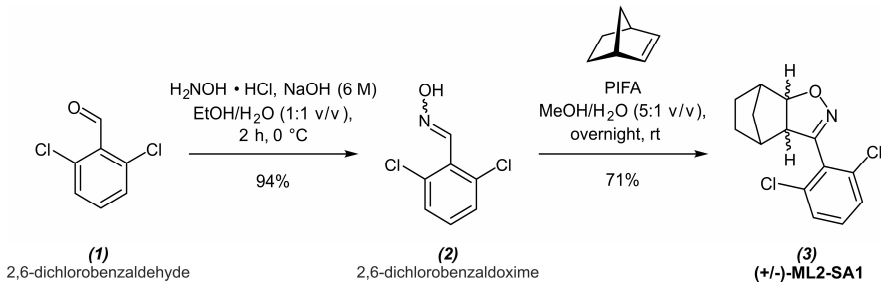

Scheme 1: Synthesis of the specific TRPML2 agonist ML2-SA1 following the protocols by McIntosh *et al*. (McIntosh et al., 2012) and Plesch *et al*. (Plesch et al., 2018). For analysis, see Fig. S1–S4.

2.3 Cell viability assay

Cell viability assays were performed using the PrestoBlue® Cell viability reagent (Thermo Fisher Scientific) according to the manufacturer's protocol. A549 cells were seeded at a density of $1x10^4$ cells/well in a flat-bottom 96-well plate and treated with ML2-SA1 and ML-SA1 dissolved in DMSO, final concentrations ranging from 12.5 µM to 200 µM for 24 h and 48 h, respectively. DMSO concentration in all wells was kept constant at 1% v/v. After an incubation period of 1 h at 37 °C with PrestoBlue® Cell viability reagent, the fluorescence of the reagent was measured in a microplate reader Infinite M1000 (Tecan Group AG). For testing of persistently HEV-infected cells, final ML2-SA1 concentrations ranging from 1 µM to 625 µM were used.

2.4 Time-of-addition experiment

A549 cells were seeded in six-well plates and infected with the ZIKV French Polynesia or Uganda isolate (MOI=1) for one hour, then unbound virus was removed. Treatment with final concentrations of 50 nM Bafilomycin A1, 100 µM ML-SA1, 100 µM ML2-SA1 or 100 µM Ribavirin was started at the respective time point (2 h before infection, during infection, 1 h, 6 h, 16 h and 22 h post infection). Complete media changes were performed during infection and 1 h post infection and compounds were refreshed, when applicable. At 24 h post infection, cells were washed once with PBS and lysed with RIPA (radio-immunoprecipitation assay) buffer for subsequent Western blot analyses.

2.5 Western blotting

A549 cells were washed with PBS, lysed with 100 µL RIPA buffer per well (including 10 µg/mL Aprotinin, 1 mM phenylmethylsulfonyl fluoride (PMSF), 25 µg/mL Leupeptin, 20 µg/mL Pepstatin (all purchased from AppliChem GmbH)) and scraped from plates. Afterwards, lysates were sonified and the protein concentration was determined using Bradford Reagent (Thermo Fisher Scientific). Samples containing 75 µg protein in SDS loading buffer were loaded on an SDS-PAGE (10% SDS) and separated using a voltage of 100 V. Afterwards, protein was transferred to a nitro-cellulose membrane by semi-dry western blotting. The membranes were blocked with 1X Roti-block (Carl Roth) for 1 h and incubated overnight with primary antibodies: anti-ZIKV E protein (Dr. Sami Akhras, Paul-Ehrlich-Institute (Akhras et al., 2019)) at a 1:500 dilution, anti-p62 (ProGen Biotechnik, 1:1,000), anti-LC3 (BIOZOL, 1:1,000), anti-pORF2 (HCD3K129, 1:2,000, raised against aa112-608 of recombinant pORF2 protein as used in a previous study (Glitscher et al., 2021a)) as well as anti-GAPDH (Santa Cruz Biotechnology, 1:2,000)

142 and anti-beta-Actin (Sigma-Aldrich, 1:10,000 dilution) as loading control for quantification. The following day,
143 membranes were washed with TBS (tris buffered saline) buffer containing 0.05% Tween and then incubated at a
144 1:10,000 dilution with secondary antibodies (IRDye® 680RD Donkey anti-Rabbit IgG, IRDye® 800CW Donkey
145 anti-Guinea Pig IgG, IRDye® 800CW Donkey anti-Mouse IgG) purchased from LI-COR Biosciences.

146

147 *2.6 RNA isolation, reverse transcription and RT-qPCR*

148 A549 cells were washed with PBS lysed with RNA-Solv® Reagent (Carl Roth) and total intracellular RNA was
149 isolated according to the manufacturer's instructions. Afterwards, DNA was digested using the RQ1 RNAse-free
150 DNase (Promega) and total RNA was transcribed into cDNA with random hexamer primer and RevertAid H Minus
151 Reverse Transcriptase (Thermo Fisher Scientific) following the manufacturer's protocol. ZIKV intracellular
152 transcripts were quantified using the Maxima SYBR Green qPCR Kit (Thermo Fisher Scientific) for real-time
153 quantitative PCR (RT-qPCR) in a LightCycler®480 System (Roche). The following primers were used for
154 determination of intracellular ZIKV genomes (fwd 5' agatcccggctgaaacactg 3', rev 5' ttgcaaggtccatctgtccc 3').
155 The housekeeping gene human ribosomal protein L27 (hRPL27, fwd 5' aaagctgtcatcgtgaagaac 3', rev 5'
156 gctgtcactttgcgggggtag 3') was used for normalization.

157

158 *2.7 Plaque assay*

159 After the treatment of A549 cells with 100 µM ML2-SA1 and infection with ZIKV French Polynesia or ZIKV
160 Uganda, supernatants were collected at the respective harvesting time point and stored at −80 °C. For plaque
161 assays, Vero cells were seeded on a six-well plate (3x 10^5 cells per well) and infected with serial dilutions of sample
162 supernatant which was centrifuged at 5 min at 5000 rpm prior to remove cell debris. The inoculum was removed
163 two hours post infection and cells were covered with 0.4% SeaPlaque™ agarose (Lonza Group AG) in medium.
164 After 20 min at room temperature (rt) for solidification of the agarose/medium mixture, cells were incubated in
165 5% CO_2 and 95% relative humidity at 37 °C for five days. Plaque visualization was performed as described
166 previously (Elgner et al., 2018).Virus titers are described as plaque forming units per mL (PFU/mL) and are
167 presented in relation to the respective DMSO control.

168

169 *2.8 Half maximal tissue culture infective dose ($TCID_{50}$)*

170 Determination of the $TCID_{50}$ was performed as described previously (Glitscher et al., 2021a). In brief, highly
171 HEV-permissive A549/D3 cells (Schemmerer et al., 2016) were infected using a serial dilution of HEV-containing
172 cell culture supernatants replicates for 96 hours. Fixation and blocking were followed by incubation with an anti-
173 pORF2 (HCD3K129) antibody, which was probed with a horseradish peroxidase-coupled secondary antibody
174 (donkey-α-rabbit IgG, GE HealthCare, 1:400). Subsequent staining was performed using 3-amino-9-ethylcarbazol.
175 The resulting $TCID_{50}$ was calculated as described previously (Ramakrishnan, 2016).

176

177 *2.9 Confocal laser scanning microscopy (cLSM) and super-resolution microscopy*

178 Cells were seeded on coverslips (1.5H) (Carl Roth) and at the desired time-point fixed with ice-cold
179 ethanol:acetone (1:1 v/v) for 10 min or 4% para-formaldehyde in PBS for 20 min at rt, respectively. For staining
180 of acidic cellular organelles, 75 nM LysoTracker™ Deep Red (Thermo Fisher Scientific) was added one hour
181 before fixation. Blocking and permeabilization were performed by addition of 5% BSA in TBS-T for 15 min at rt.
182 Samples were incubated with the following primary antibodies (anti-CD63 (Abcam, 1:200), anti-LAMP2 (R&D
183 systems, 1:100), anti-LAMP2 (BD Biosciences, 1:200), anti-E (PEI, 1:500), anti-flavivirus group antigen antibody
184 (clone D1-4G2-4-15, Sigma-Aldrich, 1:300), anti-dsRNA (SCICONS, 1:200), anti-pORF2 (HCD3K129, 1:500))
185 followed by an incubation step with the respective secondary antibodies (anti-mouse Cy™3 (1:400), anti-rabbit
186 IgG-Alexa 488 (1:1,000), anti-mouse IgG-Alexa 546 (1:1,000), anti-donkey IgG-Alexa 633 (1:1,000)) and DAPI
187 (Carl Roth) for cell nuclei visualization. For staining of intracellular cholesterol and oxysterols, 0.1 mg/mL Filipin
188 III (Sigma-Aldrich) in DMSO was added for a 30 min blocking step and incubation with secondary antibodies,
189 respectively. Coverslips were mounted with mowiol on microscope slides and analyzed using a confocal Leica
190 SP8 microscope (Leica). For super-resolution microscopy, samples were incubated with secondary antibodies
191 (STAR635P (Abberior, 1:200) and Atto594 (Merck KgaA, 1:200)), which are suitable for STED (stimulated
192 emission depletion). Image acquisition was performed on a Leica Stellaris 8 microscope system (Leica) equipped
193 with a white light laser for fluorescence excitation and three STED lasers for fluorescence inhibition using a 93x
194 objective (HC PL APO 93x/ 1.3 Glyc STED WHITE). For dual-color STED, a single STED line (775 nm) was
195 used. The pinhole was set to 1.0 AU (airy unit). For z-stacks, step sizes were set to 0.2 µm. Immunofluorescence
196 images were deconvoluted using the LasX Lightning tool. Acquisition and analysis of all images were performed
197 using the LAS X software or FIJI. For determination of the thresholded Mender's overlap coefficient (tMOC) or
198 corrected total cell fluorescence (CTCF), a minimum of eight cells were analyzed.

199

200 *2.10 ZIKV Luciferase Reporter Assay*

201 A549 cells were seeded with a density of $2x10^5$ cells/well in a 12-well plate. The following day, cells were infected
202 with 10 genome equivalents (GEs) of ZIKV Luciferase reporter virus for 4 h in the absence (DMSO only) or
203 presence of 100 µM ML2-SA1/ML-SA1. At 4 h and 24 h post infection, compounds were refreshed to ensure a
204 constant level throughout the experiment. At 48 h post infection, cells were washed, lysed with 130 µL of lysis
205 buffer (PJK GmbH) and the luciferase activity was determined using the Gaussia GLOW-Juice Kit (PJK GmbH)
206 according to the manufacturer's protocol. Luciferase activity was referred to the protein concentration of the
207 corresponding lysate which was determined by a Bradford assay beforehand.

208

209 *2.11 Statistical analyses*

210 Results are depicted as mean of at least three independent experiments ± standard deviation (SD), unless stated
211 otherwise. All data were analyzed using the software GraphPad Prism (Dotmatics) and student t test was used to
212 analyze statistical relevance. The level of statistical relevance shown in the graphs are expressed with asterisks (*)
213 that correspond to the following *p*-values: $*p < 0.05$, $**p < 0.01$, $***p < 0.001$, $****p < 0.0001$.

214

215 **3 Results**

216 *3.1 The specific TRPML2 agonist ML2-SA1 displays an antiviral effect against different ZIKV isolates*

217 A link between TRPML2 and flaviviral infections has been suggested previously (Rinkenberger and Schoggins,
218 2018), but the molecular details remained elusive. Based on the predominant localization of the cation channel in
219 the endolysosomal system, we speculated that TRPML2 may play a role in the escape, maturation, or replication
220 of endocytosed viruses and thus present a promising antiviral target (Fig. 1a).

221 To investigate TRPML2's role in ZIKV infections, we synthesized the only currently available specific TRPML2
222 agonist, ML2-SA1 (Plesch et al., 2018), according to published protocols ((McIntosh et al., 2012; Plesch et al.,
223 2018), Scheme 1, Fig. S1–S4). Upon treatment of uninfected A549 cells with up to 100 µM ML2-S1, no significant
224 cell toxicity was observed after 24 h (Fig 1b). Addition of 200 µM ML2-SA1 led to a mild but insignificant
225 decrease in the redox metabolic activity after 24 and 48 h (Fig. 1b, c). After 48 h, an increase in the percentage of
226 redox metabolic activity was detected upon addition of 12.5, 25 and 50 µM ML2-SA1 (Fig. 1c).

227 Next, we tested the antiviral potential of ML2-SA1 against ZIKV French Polynesia (H/PF/2013) and ZIKV
228 Uganda (976 Uganda). At concentrations that do not induce toxicity in A549 cells, ML2-SA1 exhibited a dose-
229 dependent reduction of the viral life cycle for both ZIKV isolates as gauged by the reduction in viral E protein
230 (Fig. 1d, e). The most pronounced effect against both isolates was observed at a concentration of 100 µM ML2-
231 SA1, which was thus used for all subsequent experiments.

232 To assess whether the reduction in the intracellular amount of E protein in ML2-SA1 treated ZIKV infected cells
233 correlates with fewer intracellular genomes, quantification of the intracellular genomes and of the released viral
234 particles was performed. For this purpose, ML2-SA1-treated A549 cells were infected with ZIKV French
235 Polynesia or Uganda and harvested 24 h post infection (hpi) and 48 hpi, respectively. For both isolates, ML2-SA1
236 strongly reduced the amount of intracellular ZIKV E protein (Fig. 2a, b), as well as intracellular ZIKV genome
237 levels (Fig. 2c, d). In accordance with this, the amount of released viral particles was also significantly diminished
238 (Fig. 2e, f).

239 Taken together, these data indicate that the TRMPL2 agonist ML2-SA1 exerts a significant antiviral effect on
240 ZIKV.

241

242 *3.2 ML2-SA1 treatment causes accumulation of ZIKV E protein in CD63-positive vesicles without leading to*
243 *enhanced ZIKV degradation*

244 With its ability to reduce ZIKV genome levels and virus titers, the TRPML2 agonist displayed an appreciable
245 antiviral effect against both tested ZIKV isolates. However, it remained unclear whether the compound interferes
246 with early infection stages (e.g. through increased lysosomal degradation of ZIKV thereby decreasing viral RNA
247 release into the cytosol) or later infection stages (i.e. impairment of viral replication). To investigate whether ML2-
248 SA1 treatment influences the pH of endolysosomal vesicles, uninfected A549 cells were subjected to ML2-SA1
249 or the V-type ATPase inhibitor Bafilomycin A1, which prevents endolysosomal acidification (Fig S5). Acidic
250 organelles were stained with the fluorescent dye LysoTracker™ and immunostaining of the lysosomal marker
251 LAMP2 was carried out. As expected, almost no LysoTracker™ positive vesicles were found in Bafilomycin A1-

252 treated cells. In contrast, ML2-SA1-treated cells displayed more and enlarged LysoTracker™-positive vesicles
253 compared to the DMSO-treated control. In addition, a drastic increase in the number as well as size of LAMP2-
254 positive vesicles was observed for ML2-SA1-treated cells. These results indicate that treatment with the TRPML2
255 agonist ML2-SA1 influences either the morphology of or fusion events within the endolysosomal system.

256 To investigate whether ML2-SA1 treatment induces accumulation of ZIKV particles in the endolysosomal system,
257 a prerequisite for a possible increase in lysosomal ZIKV degradation, we performed super-resolution microscopy
258 (Fig. 3a). Infected cells were immunostained against ZIKV E protein and human CD63, a marker for multivesicular
259 bodies (MVBs). In untreated cells, the ZIKV E protein signal was concentrated around the nucleus, in agreement
260 with the formation of ER-derived structures associated with virus replication and particle assembly (Cortese et al.,
261 2017). In ML2-SA1-treated cells, the ZIKV E protein signal was reduced and more evenly distributed across the
262 cell suggesting that replication was reduced or halted. Furthermore, ML2-SA1 treatment increased the size of
263 CD63-positive MVBs in comparison to the DMSO control. Representative 3D reconstructions revealed that ZIKV
264 E protein accumulated in these CD63-positive vesicles upon ML2-SA1 treatment.

265 A prior study suggested increased lysosomal degradation of DENV2 and ZIKV upon treatment of infected cells
266 with the unspecific TRPML-agonist ML-SA1 (Xia et al., 2020). Therefore, we investigated whether ML2-SA1-
267 treatment increases ZIKV lysosomal degradation. We incubated infected A549 cells with either ML2-SA1, the
268 membrane-permeable thiolprotease inhibitor Leupeptin, or both compounds. Leupeptin inhibits the lysosomal
269 proteases Cathepsin B, H and L thereby decreasing the proteolytic degradation of lysosomal cargo (Furuno et al.,
270 1982; Glaumann and Ahlberg, 1987). While Leupeptin alone had no effect on ZIKV E protein levels (Fig. 3b), the
271 co-treatment of ML2-SA1 and Leupeptin also showed no increase of intracellular ZIKV E protein.

272 As a control for the efficiency of lysosomal proteolysis, we thus checked whether Leupeptin application resulted
273 in the expected decrease in degradation of another lysosomal marker protein, p62 (Fig. 3b). The observed increase
274 in p62 levels upon Leupeptin addition confirms that inhibition of the acidic lysosomal proteases indeed leads to
275 reduced lysosomal protein degradation. Interestingly, the combination of Leupeptin with ML2-SA1 showed no
276 statistically significant changes in p62 levels, however when cells were treated with ML2-SA1 alone, a statistically
277 significant p62 decrease was observed in both uninfected and ZIKV Uganda-infected cells (Fig. 3b) which might
278 reflect the enhanced lysosomal capacity. Since a decrease in p62 levels has also been associated with enhanced
279 autophagy (Bjørkøy et al., 2009), we additionally looked at the increase of the LC3-II/I ratio, a second autophagy
280 marker, which would imply enhanced autophagosome formation (Kabeya et al., 2004). Here, only the treatment
281 of ZIKV French Polynesia infected cells with ML2-SA1 showed a significant effect (Fig. 3b). Together, these data
282 suggest that lysosomal degradation is not the underlying molecular mechanism of the observed antiviral effect of
283 ML2-SA1 and that enhanced autophagy plays only a minor role.

284

285 *3.3 Viral replication, and not the early ZIKV life cycle stages, are impaired by ML2-SA1 treatment*

286 Time-of-addition experiments allow the dissection which step of the viral life cycle is affected by a given
287 compound (Daelemans et al., 2011) (Fig 4a). For instance, Bafilomycin A1 restricts ZIKV entry by inhibiting the
288 V-type ATPase (Cortese et al., 2017; Sabino et al., 2019). Ribavirin, a nucleoside analogue, inhibits ZIKV

289 replication (Kamiyama et al., 2017) and the non-specific TRPML channel agonist ML-SA1 was described to
290 enhance lysosomal degradation of ZIKV (Xia et al., 2020).

291 To dissect the consequence of ML2-SA1 treatment, A549 cells were infected with the ZIKV Uganda isolate or
292 ZIKV French Polynesia and the TRPML2 agonist was added at defined time points (from -2 to +22 hpi) to capture
293 the entry and post entry phase of the viral life cycle (Fig. 4a, Fig. S6). To benchmark the effects of the TRPML2
294 channel agonist to specific events of the ZIKV life cycle stage, cells were also treated with Bafilomycin A1,
295 Ribavirin and ML-SA1. Bafilomycin A1 and Ribavirin were used at concentrations known to be non- or only
296 mildly cytotoxic, i.e. 50 nM and 100 µM, respectively (Huber et al., 2022; Sabino et al., 2019). When testing the
297 cytotoxicity of ML-SA1 in the same manner as we did for ML2-SA1, we found that neither compound displayed
298 significant cytotoxicity at a concentration of 100 µM (Fig. S7), the concentration consequently used in our time-
299 of-addition assay for both molecules.

300 In the assay, the amount of detected ZIKV E protein was normalized to the respective DMSO control (Fig. 4a,
301 black circles) to monitor the relative changes in the amount of viral E protein for each compound. In agreement
302 with the literature, we found Bafilomycin A1 to strongly suppress viral entry as reflected by the significant
303 reduction in viral E protein at early addition time points (Fig. 4a, magenta circles). Ribavirin affected the later
304 stages of the viral life cycle, 1–6 hpi, including viral replication (Fig. 4a, blue circles). Both ML2-SA1 and ML-
305 SA1 acted similar to Ribavirin and showed no antiviral effect when added during the entry process, but at later
306 stages, (Fig. 4a, green and light pink circles). No apparent differences between the experiments with ZIKV Uganda
307 or ZIKV French Polynesia isolate were observed (see Fig. S6b, c for the time-of-addition experiment with ZIKV
308 French Polynesia infected cells).

309 Since we found that ML2-SA1 did not increase the amount of released viral particles (Fig. 2e, f) and not lead to
310 enhanced ZIKV protein degradation in the endolysosomal system (Fig. 3), it seemed most likely that the observed
311 antiviral activity in the time-of-addition experiment originates from an impairment in ZIKV replication. The key
312 ZIKV replication stages (translation and cleavage of the viral polyprotein, replication of viral RNA and formation
313 of progeny ZIKV particles) take place at the ER of the host cell (Cortese et al., 2017; Rossignol et al., 2017).
314 During the formation of these viral 'replication factories', both the ER and cytoskeleton undergo massive
315 remodeling (Cortese et al., 2017; Long et al., 2020; Rossignol et al., 2017). Dense, ER-derived patches in the
316 perinuclear region which give rise to dsRNA intermediates during ZIKV replication can be observed (Cortese et
317 al., 2017). In addition, these cellular changes result in a characteristic bean-like shape formation of the host cell
318 nucleus (Cortese et al., 2017). Using confocal laser scanning microscopy, we observed the characteristic re-shaping
319 of host cell nuclei and large, dsRNA-positive patches in the perinuclear region in ZIKV-infected A549 cells (Fig.
320 4b). ML2-SA1 treatment caused a significant decrease of dsRNA in ZIKV Uganda isolate infected A549 cells.
321 Furthermore, the remaining dsRNA signal was not concentrated in distinct perinuclear patches anymore, but rather
322 evenly distributed. This suggests that the TRPML2 agonist prevented the formation of pronounced ZIKV
323 replication sites. As described above, ML2-SA1 also caused a decrease in the number of ZIKV genomes (Fig. 2c,
324 d). The notion that ML2-SA1 impairs ZIKV replication was also supported by a ZIKV *Renilla* Luciferase (*R*Luc)
325 reporter assay, which takes advantage of a *R*Luc gene fused to the viral capsid coding sequence (Shan et al., 2016).
326 Here, treatment of A549 cells with ML-SA1 or ML2-SA1 resulted in a significant decrease of luciferase activity
327 for both compounds. Interestingly, this effect was more pronounced for ML2-SA1 compared to ML-SA1 (Fig. 4c).

3.4 ML2-SA1 treatment leads to intracellular cholesterol accumulation

Although a functional role for TRPML1 in the regulation of lysosomal lipid and cholesterol trafficking has been described (Shen et al., 2012), and the cryo-electron microscopy structure of TRPML3 displays bound cholesterol molecules (Hirschi et al., 2017), no obvious connection between TRPML2 and cholesterol binding or trafficking has been established to date. Since efficient ZIKV replication requires cholesterol, which affects membrane rigidity and induces negative membrane curvature, to enable the formation or maintenance of flaviviral replication factories (Churchward et al., 2005; Steinkühler et al., 2019), we sought to explore whether addition of TRPML channel agonists may also affect intracellular cholesterol levels (Fig. 5). Using immunofluorescence, we did not observe distinct differences of cellular cholesterol distribution between infected and uninfected cells. However, upon treatment with ML2-SA1, regardless of whether cells were infected or not, pronounced cholesterol accumulation was observed in dot-like structures. In contrast, cholesterol was observed as a dispersed cytosolic signal with small punctae in untreated cells. Consistent with our previous findings (Fig. S5), ML2-SA1-treatment also enlarged the size of LAMP2-positive structures. Notably, treatment with the nonspecific TRPML channel agonist ML-SA1 had a similar effect, both with regards to cholesterol redistribution and enlarged vesicular structures. It remains to be seen whether this can solely be attributed to the molecule's action on TRPML2, or also on other TRPML channels. In summary, our results indicate that both ML-SA1 and ML2-SA1 alter the intracellular cholesterol distribution in a similar manner which may play a role in the observed antiviral effects.

3.5 ML2-SA1 enhances lysosomal degradation and decreases release of functional HEV virions

TRP channels in general and lyososmal Ca^{2+} channels specifically have been associated with viral infections beyond the flavivirus genus (Chao et al., 2023; Grimm et al., 2017; Kumar et al., 2022; Rosato et al., 2021). We thus sought to investigate whether the TRPML2 agonist ML2-SA1 is also effective against endocytosed viruses beyond ZIKV. To this end, A549 cells persistently infected with HEV were treated with ML2-SA1. HEV is the most common cause of acute viral hepatitis and treatment options are still limited (Kamar et al., 2017). Interestingly, elevated intracellular cholesterol levels promote lysosomal degradation of HEV, while reduced intracellular cholesterol levels increase viral release (Glitscher et al., 2021b). In our hands, ML2-SA1 displayed only mild cytotoxicity in persistently HEV-infected A549 cells (Fig. 6a), but significantly decreased viral titers (Fig. 6b) alongside a heavy reduction in the amount of intracellular capsid protein pORF2 (Fig. 6c). This decrease in pORF2 was confirmed on a single-cell level by cLSM analyses (Fig. 6d, e). Most importantly, there are clear signs of the capsid protein being incorporated into lysosomal structures harboring LAMP2 (Fig. 6f). This suggests an increase in lysosomal degradation of HEV upon treatment with ML2-SA1, which likely is due to the cholesterol accumulation induced by ML2-SA1 treatment (Fig. 5).

4 Discussion

Both TPCs (two-pore channels) and TRPML channels are endolysosomal cation channels which play important roles in viral infections (Chao et al., 2023; Grimm et al., 2017; Huang et al., 2021; Kumar et al., 2022; Rosato et

365 al., 2021; Sakurai et al., 2015; Santoni et al., 2020). However, their antiviral potential is not yet fully explored, in
366 part because specific functional modulators are missing. The recent synthesis and functional characterization of
367 the first TRPML2-specific agonist, ML2-SA1, by Grimm and colleagues (Plesch et al., 2018) provided us with the
368 unique opportunity to assess the role of this ion channel in the ZIKV infection process (Fig. 7).

369 For the non-specific TRPML agonist ML-SA1, which shows antiviral potential against ZIKV and DENV2 in A549
370 cells, lysosomal acidification, increased lysosomal protease activity and enhanced viral lysosomal degradation
371 were proposed to be the main mechanisms of action (Xia et al., 2020). However, the fact that ML-SA1 addresses
372 TRPML channels indiscriminately and that its mechanism of action has not yet been investigated compared to
373 reference compounds in time-of-addition experiments makes it impossible to disentangle the roles of agonist
374 treatment and the activity of individual TRPML subfamily members in flaviviral infections. Using the specific
375 TRPML2 agonist ML2-SA1, we encouragingly observed significant antiviral activity for ML2-SA1 in the same
376 concentration range previously used for ML-SA1 against DENV and ZIKV (Xia et al., 2020).

377 We also observed an increase in amount and size of acidic vesicles and accumulation of ZIKV E protein in CD63-
378 positive particles in ML2-SA1-treated cells in agreement with the prior study on ML-SA1. However, our
379 synchronized time-of-addition experiments, the use of reference compounds and the inhibition of lysosomal
380 proteases strongly suggested that the antiviral effect of this compound is not rooted in enhanced acidification and
381 viral protein degradation (Fig. 3b, Fig. 4). Rather, in our hands both ML2-SA1 and ML-SA1 affected the late
382 stages of the viral life cycle, similar to the replication inhibitor Ribavirin.

383 Interestingly, for both ML-SA1 and ML2-SA1, we also observed slightly proviral effects upon addition at early
384 infection stages. Activation of TRPML channels leads to an increased Ca^{2+} flux into the cytosol which can enhance
385 endolysosomal trafficking (Venkatachalam et al., 2015) and may therefore promote viral infection during the early
386 stages of the ZIKV life cycle. We saw that ML2-SA1 addition resulted in MVBs with an increased size (Fig. 3a)
387 which could indicate that TRPML2 activation increased vesicle trafficking and membrane fusion. This finding
388 also agrees with the observations by Rinkenberger and Schoggins using a TRPML2 overexpression system, where
389 enhanced endosomal trafficking led to a proviral effect for multiple endocytosed viruses including ZIKV
390 (Rinkenberger and Schoggins, 2018).

391 We hypothesized that the pronounced impact of ML2-SA1 on ZIKV replication may be due to the prevention of
392 the structural remodeling of the ER and impairment of the formation or maintenance of ZIKV replication factories,
393 both processes that are contingent on cholesterol (Osuna-Ramos et al., 2018). Indeed, we found an altered
394 intracellular cholesterol distribution upon treatment with ML2-SA1 (Fig. 4 and Fig. 5), thereby establishing the
395 first link between TRPML2 activity and cellular cholesterol distribution. Ca^{2+} channel modulators have previously
396 been shown to reduce ZIKV replication by interfering with intracellular cholesterol trafficking. Lacidipine for
397 example inhibits L-type calcium channels located in the plasma membrane of vascular smooth muscle cells
398 (Godfraind and Salomone, 1991; Spampinato et al., 1993) and interferes with intracellular trafficking of
399 cholesterol and other lipids thereby inhibiting ZIKV replication (Bezemer et al., 2022). Host-cholesterol is also an
400 important factor during viral entry (Glitscher and Hildt, 2021; Osuna-Ramos et al., 2018). The NPC1 inhibitor
401 U18666A inhibits both DENV entry via retarded viral trafficking in cholesterol-loaded late endosomes/lysosomes
402 and viral replication (Poh et al., 2012). During infection with the Hepatitis C virus (HCV), U18666A was shown
403 to disturb the lipid transport, which causes functional inhibition of late endosomes and formation of multilamellar

404 bodies (Elgner et al., 2016). In ZIKV-infected cells, U18666A treatment specifically inhibited viral replication
405 (Sabino et al., 2019). It is therefore tempting to speculate that changes in cellular cholesterol distribution are also
406 the molecular basis for the observed antiviral effect of ML2-SA1. Such a broad mechanism of action would imply
407 that the antiviral potential of ML2-SA1 does not end with ZIKV but should extend to other viruses reliant on
408 cholesterol. Indeed, many viruses depend on cholesterol during viral entry (Glitscher and Hildt, 2021; Osuna-
409 Ramos et al., 2018) and elevation of intracellular cholesterol was successfully used to reduce infection with HEV
410 by increasing lysosomal degradation of viral pORF2 (Glitscher et al., 2021b). Encouragingly, ML2-SA1 also
411 showed antiviral activity against HEV (Fig. 6).

412 In this study we saw that the TRPML2-specific agonist ML2-SA1 induced a pronounced antiviral effect against
413 two ZIKV isolates, one representative of the African lineage (ZIKV Uganda) and one representative of the Asian
414 lineage (French Polynesia). ML2-SA1 treatment did not induce increased lysosomal ZIKV degradation, but rather
415 inhibited viral replication, possibly due to an altered intracellular cholesterol distribution. Due to the high similarity
416 of the life cycle of flaviviruses, it seems likely that ML2-SA1 also shows antiviral potential against other
417 flaviviruses such as DENV, WNV and yellow fever virus (YFV). It will be interesting to investigate the connection
418 between TRPML2, the other TRPML channels, viral infections, and host cell cholesterol distribution in more
419 detail. It may be well conceivable that all members of the TRPML channel subfamily play central regulatory roles
420 within the lipid distribution networks of the cell and that this functionality could provide a lever for the
421 development of novel antiviral drugs targeting endolysosomal TRP ion channels.

422

423 ***Author contributions***

424 Experiment design, K.K.S, M.G., E.H., and U.A.H.; cell viability assays, western blotting, K.K.S., S.P., and M.G.,
425 time-of-addition experiment, RT-qPCR and plaque assay, K.K.S., $TCID_{50}$, S.P. and M.G.; microscopy, K.K.S.,
426 D.B. and M.G.; ZIKV Luciferase reporter assay, R.M. and D.B.; organic synthesis, K.S.; data analysis and
427 interpretation, K.K.S., M.G., D. B., E.H. and U.A.H.; writing of the paper, K.K.S., M.G., E.H. and U.A.H. with
428 contributions from all authors; study supervision, T.S., E.H., and U.A.H.

429

430 ***Declaration of competing interest***

431 The authors declare no conflict of interest.

432

433 ***Acknowledgements***

434 We thank Gert Carra for technical support, and Charlotte Guhl for fruitful discussions. K.K.S. acknowledges a
435 PhD fellowship of the Max Planck Graduate Center (MPGC). U.A.H. acknowledges funding through a Boehringer
436 Ingelheim Foundation Exploration Grant. This work was supported by the Deutsche Forschungsgemeinschaft
437 (DFG, German Research Foundation) through the collaborative research center 1507 "Membrane-associated
438 Protein Assemblies, Machineries, and Supercomplexes" (Project ID 450648163), the collaborative research center
439 1278 "Polymer-based nanoparticle libraries for targeted anti-inflammatory strategies" (project ID 316213987) and
440 the Cluster of Excellence "Balance of the Microverse" (EXC 2051—Project-ID 390713860) (to U.A.H.). E.H.

obtained a grant by the LOEWE Center DRUID (Novel Drug Targets against Poverty-Related and Neglected Tropical Infectious Diseases; Project D2).

Abbreviations

aa	amino acids
cLSM	confocal laser scanning microscopy
CTCF	corrected total cell fluorescence
CV	coefficient of variation
DENV	Dengue virus
DMSO	dimethyl sulfoxide
E protein	envelope protein
FBS	fetal bovine serum
GEs	genome equivalents
HCV	Hepatitis C virus
HEV	Hepatitis E virus
hpi	hours post infection
IAV	Influenza A virus
ML2-SA1	mucolipin 2 synthetic agonist 1
ML-SA1	mucolipin synthetic agonist 1
MOI	multiplicity of infection
MVB	multivesicular body
PBS	phosphate buffered saline
PFU	plaque forming units
PIFA	(bis(trifluoroacetoxy)iodo)benzene
PMSF	phenylmethylsulfonyl fluoride
Renilla Luciferase	*R*luc
RIPA	radio-immunoprecipitation assay
rt	room temperature
RT-qPCR	real-time quantitative polymerase chain reaction
SD	standard deviation
STED	stimulated emission depletion
TBS	tris buffered saline
$TCID_{50}$	half maximal tissue culture infective dose
tMOC	thresholded Mender's overlap coefficient
TPC	two-pore channels
TRPML	transient receptor potential mucolipin
WNV	West Nile virus
YFV	yellow fever virus
ZIKV FP	ZIKV French Polynesia isolate
ZIKV U	ZIKV Uganda isolate

481 ZIKV Zika virus

482

483 ***References***

484 Agrelli, A., de Moura, R.R., Crovella, S., Brandão, L.A.C., 2019. ZIKA virus entry mechanisms in human cells.
485 Infection, Genetics and Evolution 69, 22–29. https://doi.org/https://doi.org/10.1016/j.meegid.2019.01.018

486 Akhras, S., Herrlein, M.-L., Elgner, F., Holzhauser, T., Hildt, E., 2019. ZIKV Envelope Domain-Specific
487 Antibodies: Production, Purification and Characterization. Viruses 11. https://doi.org/10.3390/v11080748

488 Bezemer, B., van Cleef, K.W.R., Overheul, G.J., Miesen, P., van Rij, R.P., 2022. The calcium channel inhibitor
489 lacidipine inhibits Zika virus replication in neural progenitor cells. Antiviral Res 202, 105313.
490 https://doi.org/10.1016/j.antiviral.2022.105313

491 Bjørkøy, G., Lamark, T., Pankiv, S., Øvervatn, A., Brech, A., Johansen, T., 2009. Monitoring autophagic
492 degradation of p62/SQSTM1. Methods Enzymol 452, 181–197. https://doi.org/10.1016/S0076-
493 6879(08)03612-4

494 Chao, Y.-K., Chang, S.-Y., Grimm, C., 2023. Endo-Lysosomal Cation Channels and Infectious Diseases, in:
495 Pedersen, S.H.F., Barber, D.L. (Eds.), Organelles in Disease. Springer International Publishing, Cham, pp.
496 259–276. https://doi.org/10.1007/112_2020_31

497 Chen, C.-C., Keller, M., Hess, M., Schiffmann, R., Urban, N., Wolfgardt, A., Schaefer, M., Bracher, F., Biel, M.,
498 Wahl-Schott, C., Grimm, C., 2014. A small molecule restores function to TRPML1 mutant isoforms
499 responsible for mucolipidosis type IV. Nat Commun 5, 4681. https://doi.org/10.1038/ncomms5681

500 Churchward, M.A., Rogasevskaia, T., Höfgen, J., Bau, J., Coorssen, J.R., 2005. Cholesterol facilitates the native
501 mechanism of Ca2+-triggered membrane fusion. J Cell Sci 118, 4833–4848.
502 https://doi.org/10.1242/jcs.02601

503 Cortese, M., Goellner, S., Acosta, E.G., Neufeldt, C.J., Oleksiuk, O., Lampe, M., Haselmann, U., Funaya, C.,
504 Schieber, N., Ronchi, P., Schorb, M., Pruunsild, P., Schwab, Y., Chatel-Chaix, L., Ruggieri, A.,
505 Bartenschlager, R., 2017. Ultrastructural Characterization of Zika Virus Replication Factories. Cell Rep 18,
506 2113–2123. https://doi.org/10.1016/j.celrep.2017.02.014

507 Daelemans, D., Pauwels, R., De Clercq, E., Pannecouque, C., 2011. A time-of–drug addition approach to target
508 identification of antiviral compounds. Nat Protoc 6, 925–933. https://doi.org/10.1038/nprot.2011.330

509 Dai, L., Song, J., Lu, X., Deng, Y.-Q., Musyoki, A.M., Cheng, H., Zhang, Y., Yuan, Y., Song, H., Haywood, J.,
510 Xiao, H., Yan, J., Shi, Y., Qin, C.-F., Qi, J., Gao, G.F., 2016. Structures of the Zika Virus Envelope Protein
511 and Its Complex with a Flavivirus Broadly Protective Antibody. Cell Host Microbe 19, 696–704.
512 https://doi.org/10.1016/j.chom.2016.04.013

513 Elgner, F., Ren, H., Medvedev, R., Ploen, D., Himmelsbach, K., Boller, K., Hildt, E., 2016. The Intracellular
514 Cholesterol Transport Inhibitor U18666A Inhibits the Exosome-Dependent Release of Mature Hepatitis C
515 Virus. J Virol 90, 11181–11196. https://doi.org/10.1128/jvi.01053-16

516 Elgner, F., Sabino, C., Basic, M., Ploen, D., Grünweller, A., Hildt, E., 2018. Inhibition of Zika Virus Replication
517 by Silvestrol. Viruses 10. https://doi.org/10.3390/v10040149

518 Furuno, K., Ishikawa, T., Kato, K., 1982. Appearance of autolysosomes in rat liver after leupeptin treatment. J
519 Biochem 91, 1485–1494. https://doi.org/10.1093/oxfordjournals.jbchem.a133840

520 García-Añoveros, J., Wiwatpanit, T., 2014. TRPML2 and mucolipin evolution. Handb Exp Pharmacol 222, 647–
521 658. https://doi.org/10.1007/978-3-642-54215-2_25

522 Glaumann, H., Ahlberg, J., 1987. Comparison of different autophagic vacuoles with regard to
523 ultrastructure, enzymatic composition, and degradation capacity--formation of crinosomes. Exp Mol Pathol
524 47, 346–362. https://doi.org/10.1016/0014-4800(87)90018-9

525 Glitscher, M., Hildt, E., 2021. Endosomal Cholesterol in Viral Infections - A Common Denominator? Front
526 Physiol 12, 750544. https://doi.org/10.3389/fphys.2021.750544

527 Glitscher, M., Himmelsbach, K., Woytinek, K., Schollmeier, A., Johne, R., Praefcke, G.J.K., Hildt, E., 2021a.
528 Identification of the Interferon-Inducible GTPase GBP1 as a Major Restriction Factor for Hepatitis E Virus.
529 J Virol 95, 10.1128/jvi.01564-20. https://doi.org/10.1128/jvi.01564-20

530 Glitscher, M., Martín, D.H., Woytinek, K., Schmidt, B., Tabari, D., Scholl, C., Stingl, J.C., Seelow, E., Choi, M.,
531 Hildt, E., 2021b. Targeting Cholesterol Metabolism as Efficient Antiviral Strategy Against the Hepatitis E
532 Virus. Cell Mol Gastroenterol Hepatol 12, 159–180. https://doi.org/10.1016/j.jcmgh.2021.02.002

533 Godfraind, T., Salomone, S., 1991. Functional interaction of lacidipine with calcium channels in vascular
534 smooth muscle. J Cardiovasc Pharmacol 18 Suppl 1, S1-6. https://doi.org/10.1097/00005344-199102001-
535 00001

536 Goretzki, B., Guhl, C., Tebbe, F., Harder, J.-M., Hellmich, U.A., 2021. Unstructural Biology of TRP Ion Channels:
537 The Role of Intrinsically Disordered Regions in Channel Function and Regulation. J Mol Biol 433, 166931.
538 https://doi.org/https://doi.org/10.1016/j.jmb.2021.166931

539 Grimm, C., Butz, E., Chen, C.-C., Wahl-Schott, C., Biel, M., 2017. From mucolipidosis type IV to Ebola: TRPML
540 and two-pore channels at the crossroads of endo-lysosomal trafficking and disease. Cell Calcium 67, 148–
541 155. https://doi.org/https://doi.org/10.1016/j.ceca.2017.04.003

542 Grimm, C., Jörs, S., Guo, Z., Obukhov, A.G., Heller, S., 2012. Constitutive activity of TRPML2 and TRPML3
543 channels versus activation by low extracellular sodium and small molecules. J Biol Chem 287, 22701–
544 22708. https://doi.org/10.1074/jbc.M112.368876

545 Grimm, C., Jörs, S., Saldanha, S.A., Obukhov, A.G., Pan, B., Oshima, K., Cuajungco, M.P., Chase, P., Hodder,
546 P., Heller, S., 2010. Small molecule activators of TRPML3. Chem Biol 17, 135–148.
547 https://doi.org/10.1016/j.chembiol.2009.12.016

548 Hirschi, M., Herzik Jr, M.A., Wie, J., Suo, Y., Borschel, W.F., Ren, D., Lander, G.C., Lee, S.-Y., 2017. Cryo-
549 electron microscopy structure of the lysosomal calcium-permeable channel TRPML3. Nature 550, 411–414.
550 https://doi.org/10.1038/nature24055

551 Huang, L., Yuen, T.T.-T., Ye, Z., Liu, S., Zhang, G., Chu, H., Yue, J., 2021. Berbamine inhibits SARS-CoV-2
552 infection by compromising TRPMLs-mediated endolysosomal trafficking of ACE2. Signal Transduct
553 Target Ther. https://doi.org/10.1038/s41392-021-00584-6

554 Huber, S., Braun, N.J., Schmacke, L.C., Quek, J.P., Murra, R., Bender, D., Hildt, E., Luo, D., Heine, A.,
555 Steinmetzer, T., 2022. Structure-Based Optimization and Characterization of Macrocyclic Zika Virus NS2B-
556 NS3 Protease Inhibitors. J Med Chem 65, 6555–6572. https://doi.org/10.1021/acs.jmedchem.1c01860

557 Johne, R., Reetz, J., Ulrich, R.G., Machnowska, P., Sachsenröder, J., Nickel, P., Hofmann, J., 2014. An ORF1-
558 rearranged hepatitis E virus derived from a chronically infected patient efficiently replicates in cell culture.
559 J Viral Hepat 21, 447–456. https://doi.org/https://doi.org/10.1111/jvh.12157

560 Kabeya, Y., Mizushima, N., Yamamoto, A., Oshitani-Okamoto, S., Ohsumi, Y., Yoshimori, T., 2004. LC3,
561 GABARAP and GATE16 localize to autophagosomal membrane depending on form-II formation. J Cell Sci
562 117, 2805–2812. https://doi.org/10.1242/jcs.01131

563 Kamar, N., Izopet, J., Pavio, N., Aggarwal, R., Labrique, A., Wedemeyer, H., Dalton, H.R., 2017. Hepatitis E
564 virus infection. Nat Rev Dis Primers 3, 17086. https://doi.org/10.1038/nrdp.2017.86

565 Kamiyama, N., Soma, R., Hidano, S., Watanabe, K., Umekita, H., Fukuda, C., Noguchi, K., Gendo, Y., Ozaki, T.,
566 Sonoda, A., Sachi, N., Runtuwene, L.R., Miura, Y., Matsubara, E., Tajima, S., Takasaki, T., Eshita, Y.,
567 Kobayashi, T., 2017. Ribavirin inhibits Zika virus (ZIKV) replication in vitro and suppresses viremia in
568 ZIKV-infected STAT1-deficient mice. Antiviral Res 146, 1–11.
569 https://doi.org/https://doi.org/10.1016/j.antiviral.2017.08.007

570 Kim, H.J., Soyombo, A.A., Tjon-Kon-Sang, S., So, I., Muallem, S., 2009. The Ca(2+) channel TRPML3 regulates
571 membrane trafficking and autophagy. Traffic 10, 1157–1167. https://doi.org/10.1111/j.1600-
572 0854.2009.00924.x

573 Kumar, P.S., Radhakrishnan, A., Mukherjee, T., Khamaru, S., Chattopadhyay, Soma, Chattopadhyay, Subhasis,
574 2022. Understanding the role of Ca(2+) via transient receptor potential (TRP) channel in viral infection:
575 Implications in developing future antiviral strategies. Virus Res 323, 198992.
576 https://doi.org/10.1016/j.virusres.2022.198992

577 Lanford, R.E., Guerra, B., Lee, H., Chavez, D., Brasky, K.M., Bigger, C.B., 2006. Genomic response to interferon-
578 alpha in chimpanzees: implications of rapid downregulation for hepatitis C kinetics. Hepatology 43, 961–
579 972. https://doi.org/10.1002/hep.21167

580 Li, M., Zhang, W.K., Benvin, N.M., Zhou, X., Su, D., Li, H., Wang, S., Michailidis, I.E., Tong, L., Li, X., Yang,
581 J., 2017. Structural basis of dual Ca(2+)/pH regulation of the endolysosomal TRPML1 channel. Nat Struct
582 Mol Biol 24, 205–213. https://doi.org/10.1038/nsmb.3362

583 Long, R.K.M., Moriarty, K.P., Cardoen, B., Gao, G., Vogl, A.W., Jean, F., Hamarneh, G., Nabi, I.R., 2020. Super
584 resolution microscopy and deep learning identify Zika virus reorganization of the endoplasmic reticulum.
585 Sci Rep 10, 20937. https://doi.org/10.1038/s41598-020-77170-3

586 McIntosh, M.L., Naffziger, M.R., Ashburn, B.O., Zakharov, L.N., Carter, R.G., 2012. Highly regioselective nitrile
587 oxide dipolar cycloadditions with ortho-nitrophenyl alkynes. Org Biomol Chem 10, 9204–9213.
588 https://doi.org/10.1039/c2ob26267c

589 Medina, D.L., Di Paola, S., Peluso, I., Armani, A., De Stefani, D., Venditti, R., Montefusco, S., Scotto-Rosato, A.,
590 Prezioso, C., Forrester, A., Settembre, C., Wang, W., Gao, Q., Xu, H., Sandri, M., Rizzuto, R., De Matteis,
591 M.A., Ballabio, A., 2015. Lysosomal calcium signalling regulates autophagy through calcineurin and TFEB.
592 Nat Cell Biol 17, 288–299. https://doi.org/10.1038/ncb3114

593 Nour, A.M., Li, Y., Wolenski, J., Modis, Y., 2013. Viral membrane fusion and nucleocapsid delivery into the
594 cytoplasm are distinct events in some flaviviruses. PLoS Pathog 9, e1003585.
595 https://doi.org/10.1371/journal.ppat.1003585

596 Osuna-Ramos, J.F., Reyes-Ruiz, J.M., Del Ángel, R.M., 2018. The Role of Host Cholesterol During Flavivirus
597 Infection. Front Cell Infect Microbiol 8, 388. https://doi.org/10.3389/fcimb.2018.00388

598 Plesch, E., Chen, C.-C., Butz, E., Scotto Rosato, A., Krogsaeter, E.K., Yinan, H., Bartel, K., Keller, M., Robaa,
599 D., Teupser, D., Holdt, L.M., Vollmar, A.M., Sippl, W., Puertollano, R., Medina, D., Biel, M., Wahl-Schott,
600 C., Bracher, F., Grimm, C., 2018. Selective agonist of TRPML2 reveals direct role in chemokine release
601 from innate immune cells. Elife 7. https://doi.org/10.7554/eLife.39720

602 Poh, M.K., Shui, G., Xie, X., Shi, P.-Y., Wenk, M.R., Gu, F., 2012. U18666A, an intra-cellular cholesterol
603 transport inhibitor, inhibits dengue virus entry and replication. Antiviral Res 93, 191–198.
604 https://doi.org/https://doi.org/10.1016/j.antiviral.2011.11.014

605 Ramakrishnan, M.A., 2016. Determination of 50% endpoint titer using a simple formula. World J Virol 5, 85–86.
606 https://doi.org/10.5501/wjv.v5.i2.85

607 Rinkenberger, N., Schoggins, J.W., 2018. Mucolipin-2 Cation Channel Increases Trafficking Efficiency of
608 Endocytosed Viruses. mBio 9. https://doi.org/10.1128/mBio.02314-17

609 Rosato, A.S., Tang, R., Grimm, C., 2021. Two-pore and TRPML cation channels: Regulators of phagocytosis,
610 autophagy and lysosomal exocytosis. Pharmacol Ther 220, 107713.
611 https://doi.org/https://doi.org/10.1016/j.pharmthera.2020.107713

612 Rossignol, E.D., Peters, K.N., Connor, J.H., Bullitt, E., 2017. Zika virus induced cellular remodelling. Cell
613 Microbiol 19. https://doi.org/10.1111/cmi.12740

614 Sabino, C., Basic, M., Bender, D., Elgner, F., Himmelsbach, K., Hildt, E., 2019. Bafilomycin A1 and U18666A
615 Efficiently Impair ZIKV Infection. Viruses 11. https://doi.org/10.3390/v11060524

616 Sakurai, Y., Kolokoltsov, A.A., Chen, C.-C., Tidwell, M.W., Bauta, W.E., Klugbauer, N., Grimm, C., Wahl-
617 Schott, C., Biel, M., Davey, R.A., 2015. Two-pore channels control Ebola virus host cell entry and are drug
618 targets for disease treatment. Science (1979) 347, 995–998. https://doi.org/10.1126/science.1258758

619 Samie, M., Wang, X., Zhang, X., Goschka, A., Li, X., Cheng, X., Gregg, E., Azar, M., Zhuo, Y., Garrity, A.G.,
620 Gao, Q., Slaugenhaupt, S., Pickel, J., Zolov, S.N., Weisman, L.S., Lenk, G.M., Titus, S., Bryant-Genevier,
621 M., Southall, N., Juan, M., Ferrer, M., Xu, H., 2013. A TRP channel in the lysosome regulates large particle
622 phagocytosis via focal exocytosis. Dev Cell 26, 511–524. https://doi.org/10.1016/j.devcel.2013.08.003

623 Santoni, G., Morelli, M.B., Amantini, C., Nabissi, M., Santoni, M., Santoni, A., 2020. Involvement of the TRPML
624 Mucolipin Channels in Viral Infections and Anti-viral Innate Immune Responses . Frontiers in
625 Immunology .

626 Schemmerer, M., Apelt, S., Trojnar, E., Ulrich, R.G., Wenzel, J.J., Johne, R., 2016. Enhanced Replication of
627 Hepatitis E Virus Strain 47832c in an A549-Derived Subclonal Cell Line. Viruses 8.
628 https://doi.org/10.3390/v8100267

629 Schoggins, J.W., 2019. Interferon-Stimulated Genes: What Do They All Do? Annu Rev Virol 6, 567–584.
630 https://doi.org/10.1146/annurev-virology-092818-015756

631 Schuler-Faccini, L., Ribeiro, E.M., Feitosa, I.M.L., Horovitz, D.D.G., Cavalcanti, D.P., Pessoa, A., Doriqui,
632 M.J.R., Neri, J.I., Neto, J.M. de P., Wanderley, H.Y.C., Cernach, M., El-Husny, A.S., Pone, M.V.S., Serao,
633 C.L.C., Sanseverino, M.T. V, 2016. Possible Association Between Zika Virus Infection and Microcephaly -
634 Brazil, 2015. MMWR Morb Mortal Wkly Rep 65, 59–62. https://doi.org/10.15585/mmwr.mm6503e2

635 Shan, C., Xie, X., Muruato, A.E., Rossi, S.L., Roundy, C.M., Azar, S.R., Yang, Y., Tesh, R.B., Bourne, N., Barrett,
636 A.D., Vasilakis, N., Weaver, S.C., Shi, P.-Y., 2016. An Infectious cDNA Clone of Zika Virus to Study Viral
637 Virulence, Mosquito Transmission, and Antiviral Inhibitors. Cell Host Microbe 19, 891–900.
638 https://doi.org/10.1016/j.chom.2016.05.004

639 Shen, D., Wang, X., Li, X., Zhang, X., Yao, Z., Dibble, S., Dong, X., Yu, T., Lieberman, A.P., Showalter, H.D.,
640 Xu, H., 2012. Lipid storage disorders block lysosomal trafficking by inhibiting a TRP channel and
641 lysosomal calcium release. Nat Commun 3, 731. https://doi.org/10.1038/ncomms1735

642 Spampinato, S., Bachetti, T., Carboni, L., Ratti, E., Van Amsterdam, F.T., Ferri, S., 1993. Ca2+ channel blocking
643 activity of lacidipine and amlodipine in A7r5 vascular smooth muscle cells. Eur J Pharmacol 244, 139–144.
644 https://doi.org/10.1016/0922-4106(93)90019-6

645 Spix, B., Chao, Y.-K., Abrahamian, C., Chen, C.-C., Grimm, C., 2020. TRPML Cation Channels in Inflammation
646 and Immunity. Front Immunol 11, 225. https://doi.org/10.3389/fimmu.2020.00225

647 Steinkühler, J., Sezgin, E., Urbančič, I., Eggeling, C., Dimova, R., 2019. Mechanical properties of plasma
648 membrane vesicles correlate with lipid order, viscosity and cell density. Commun Biol 2, 337.
649 https://doi.org/10.1038/s42003-019-0583-3

650 Sun, L., Hua, Y., Vergarajauregui, S., Diab, H.I., Puertollano, R., 2015. Novel Role of TRPML2 in the Regulation
651 of the Innate Immune Response. J Immunol 195, 4922–4932. https://doi.org/10.4049/jimmunol.1500163

652 Sun, M., Goldin, E., Stahl, S., Falardeau, J.L., Kennedy, J.C., Acierno, J.S.J., Bove, C., Kaneski, C.R., Nagle, J.,
653 Bromley, M.C., Colman, M., Schiffmann, R., Slaugenhaupt, S.A., 2000. Mucolipidosis type IV is caused by
654 mutations in a gene encoding a novel transient receptor potential channel. Hum Mol Genet 9, 2471–2478.
655 https://doi.org/10.1093/hmg/9.17.2471

656 Venkatachalam, K., Wong, C.-O., Zhu, M.X., 2015. The role of TRPMLs in endolysosomal trafficking and
657 function. Cell Calcium 58, 48–56. https://doi.org/10.1016/j.ceca.2014.10.008

658 Vergarajauregui, S., Connelly, P.S., Daniels, M.P., Puertollano, R., 2008. Autophagic dysfunction in
659 mucolipidosis type IV patients. Hum Mol Genet 17, 2723–2737. https://doi.org/10.1093/hmg/ddn174

660 Viet, K.K., Wagner, A., Schwickert, K., Hellwig, N., Brennich, M., Bader, N., Schirmeister, T., Morgner, N.,
661 Schindelin, H., Hellmich, U.A., 2019. Structure of the Human TRPML2 Ion Channel

662 Extracytosolic/Lumenal Domain. Structure 27, 1246-1257.e5.
663 https://doi.org/https://doi.org/10.1016/j.str.2019.04.016

664 Xia, Z., Ren, Y., Li, S., Xu, J., Wu, Y., Cao, Z., 2021. ML-SA1 and SN-2 inhibit endocytosed viruses through
665 regulating TRPML channel expression and activity. Antiviral Res 195, 105193.
666 https://doi.org/10.1016/j.antiviral.2021.105193

667 Xia, Z., Wang, L., Li, S., Tang, W., Sun, F., Wu, Y., Miao, L., Cao, Z., 2020. ML-SA1, a selective TRPML agonist,
668 inhibits DENV2 and ZIKV by promoting lysosomal acidification and protease activity. Antiviral Res 182,
669 104922. https://doi.org/10.1016/j.antiviral.2020.104922

670 Zeevi, D.A., Frumkin, A., Offen-Glasner, V., Kogot-Levin, A., Bach, G., 2009. A potentially dynamic lysosomal
671 role for the endogenous TRPML proteins. J Pathol 219, 153–162.
672 https://doi.org/https://doi.org/10.1002/path.2587

673

674

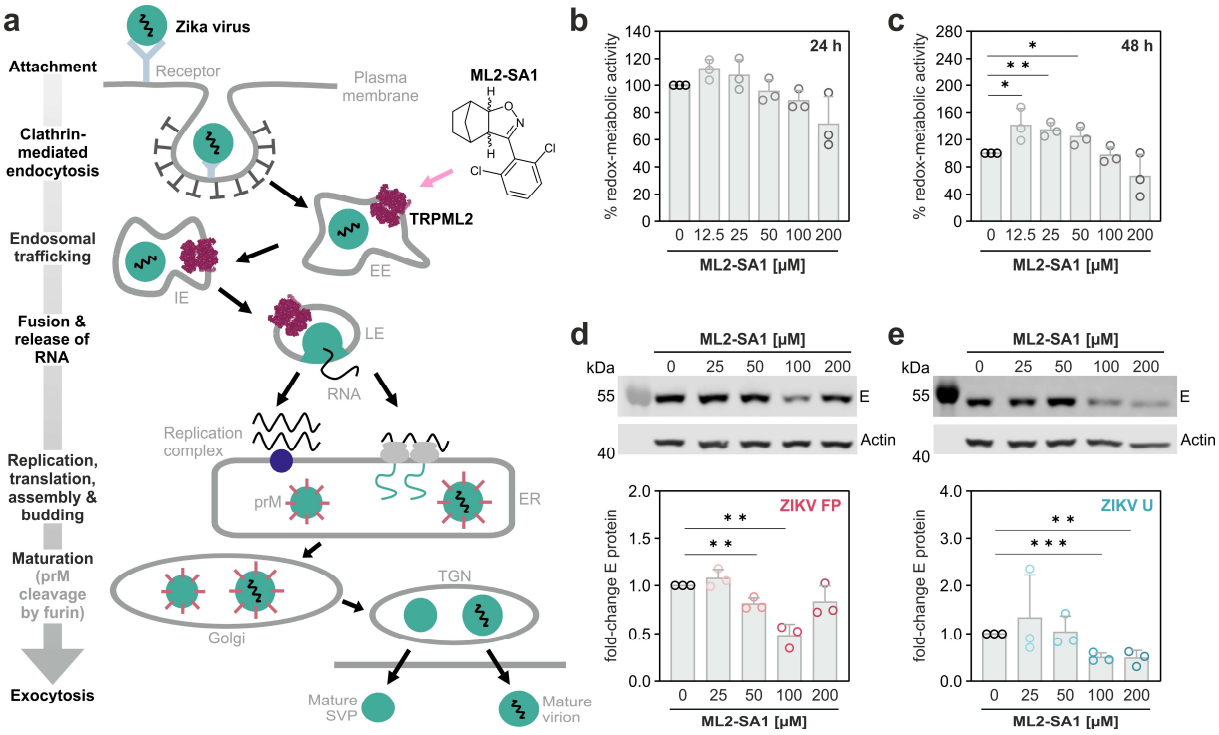

Figure 2: The specific TRPML2 agonist ML2-SA1 inhibits infection with two ZIKV isolates in a dose-dependent manner. (a) Schematic overview of the Zika virus life cycle. **Abbreviations:** EE: early endosome, IE: intermediate endosome, LE: late endosome, ER: endoplasmic reticulum, prM: pre-membrane protein, TGN: trans-Golgi network, SVP: subviral particle. **(b, c)** Cell viability of A549 cells upon treatment with 12.5 µM to 200 µM ML2-SA1 after 24 h (b) and 48 h (c) assessed with the PrestoBlue® assay. Values are expressed as % of intact cells normalized to the experimental control. **(d, e)** Relative fold-changes in ZIKV E protein of infected A549 cells treated with varying concentrations of ML2-SA1. ML2-SA1 was added to A549 cells two hours before infection (MOI = 1 with ZIKV French Polynesia (FP, H/PF/2013) or ZIKV Uganda (U, 976 Uganda)) and afterwards the compound was refreshed during every medium change to assure its constant presence. Cells were harvested 24 hpi followed by Western blotting to detect viral E protein. Data are normalized to the respective DMSO control and are expressed as mean ± SD from $n = 3$ biological replicates, a representative blot is shown. Statistical significance was determined by using an unpaired *t*-test. *$p < 0.05$, **$p < 0.01$, ***$p < 0.001$, ****$p < 0.0001$.

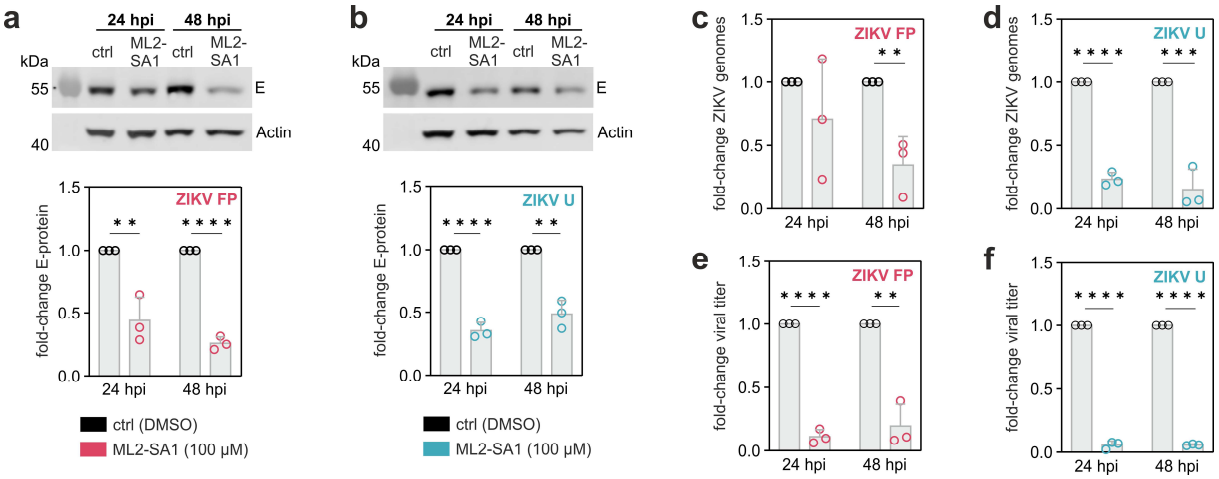

Figure 3: ML2-SA1 reduces intracellular ZIKV E protein and genome levels as well as the amount of released viral particles. A549 cells were treated with 100 µM ML2-SA1 for 2 h, then infected with the ZIKV French Polynesia (H/PF/2013) or ZIKV Uganda (976 Uganda) isolate (MOI = 1) and harvested 24 hpi and 48 hpi. (**a**, **b**) Relative fold-change of viral E protein determined by Western Blot. A representative Western Blot is shown above. (**c**, **d**) Relative fold-change in intracellular ZIKV genomes assessed via RT-qPCR. (**e**, **f**) Amount of released infectious ZIKV particles is determined using a plaque assay. Data are normalized to the respective DMSO control for each time point and are expressed as mean ± SD from $n = 3$ biological replicates. Statistical significance was determined by using an unpaired *t*-test. *$p < 0.05$, **$p < 0.01$, ***$p < 0.001$, ****$p < 0.0001$.

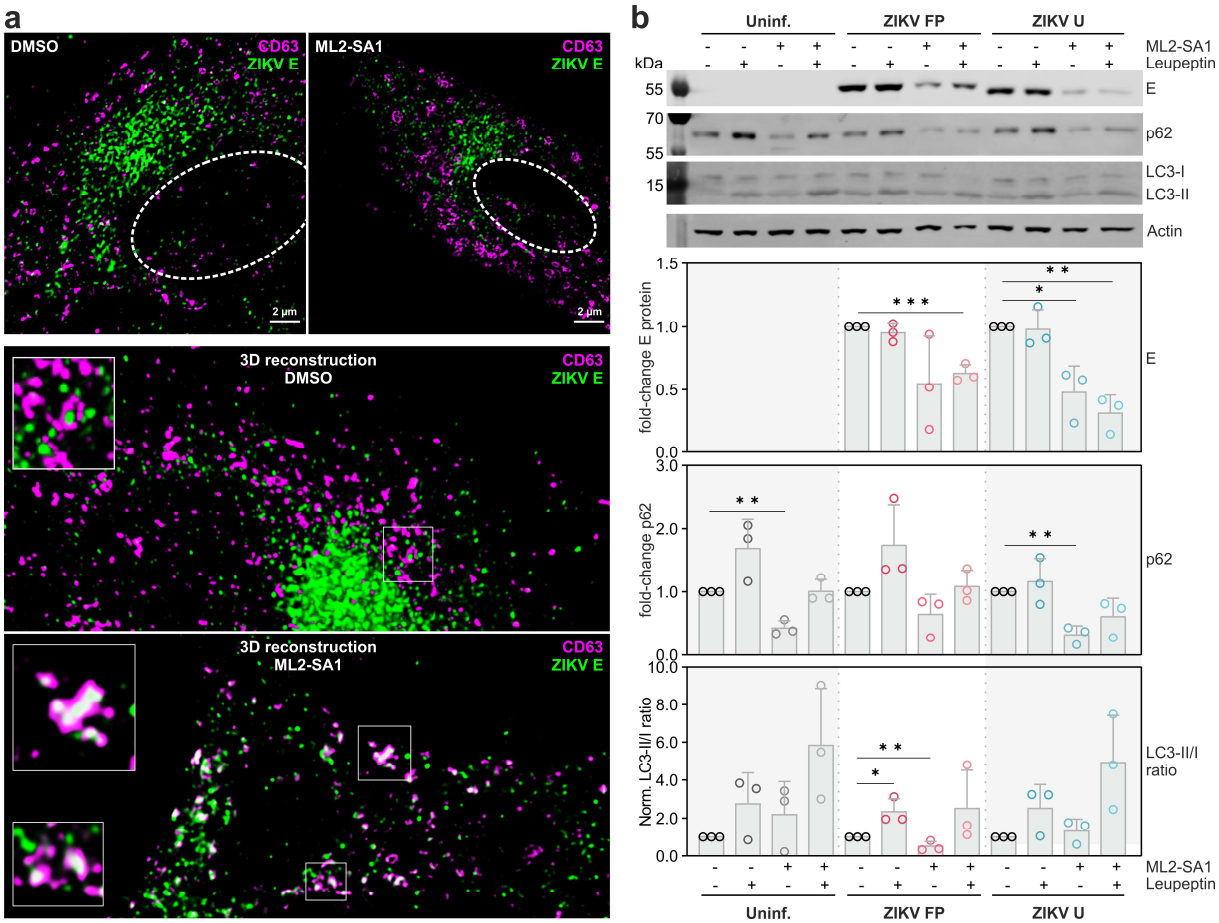

Figure 4: TRPML2 agonist treatment leads to ZIKV E protein accumulation in multivesicular bodies but not increased lysosomal degradation. (a) Representative super resolution microscopy images of A549 cells treated with DMSO (left) or 100 µM ML2-SA1 in DMSO (right) and infected with ZIKV Uganda (976 Uganda). Cells were fixed 24 hpi for immunostaining with antibodies against ZIKV E protein (green) and CD63 (magenta). The position of the cell nucleus is indicated by a dotted circle. Scale bar: 2 µm. Representative 3D reconstructions are shown below. **(b)** Relative fold-change of E protein, p62 and LC3 determined by Western Blotting. Representative Western Blots are shown above. A549 cells were treated with 100 µM ML2-SA1 and/or 0.1 mg/mL Leupeptin for 2 h before infection. Cells were infected (MOI = 1) with the ZIKV French Polynesia (H/PF/2013) and ZIKV Uganda (976 Uganda) isolate and harvested 24 hpi and 48 hpi. Data are normalized to the respective DMSO control and are expressed as mean ± SD from n = 3 biological replicates. Statistical significance was determined by using an unpaired t-test. *$p < 0.05$, **$p < 0.01$, ***$p < 0.001$, ****$p < 0.0001$.

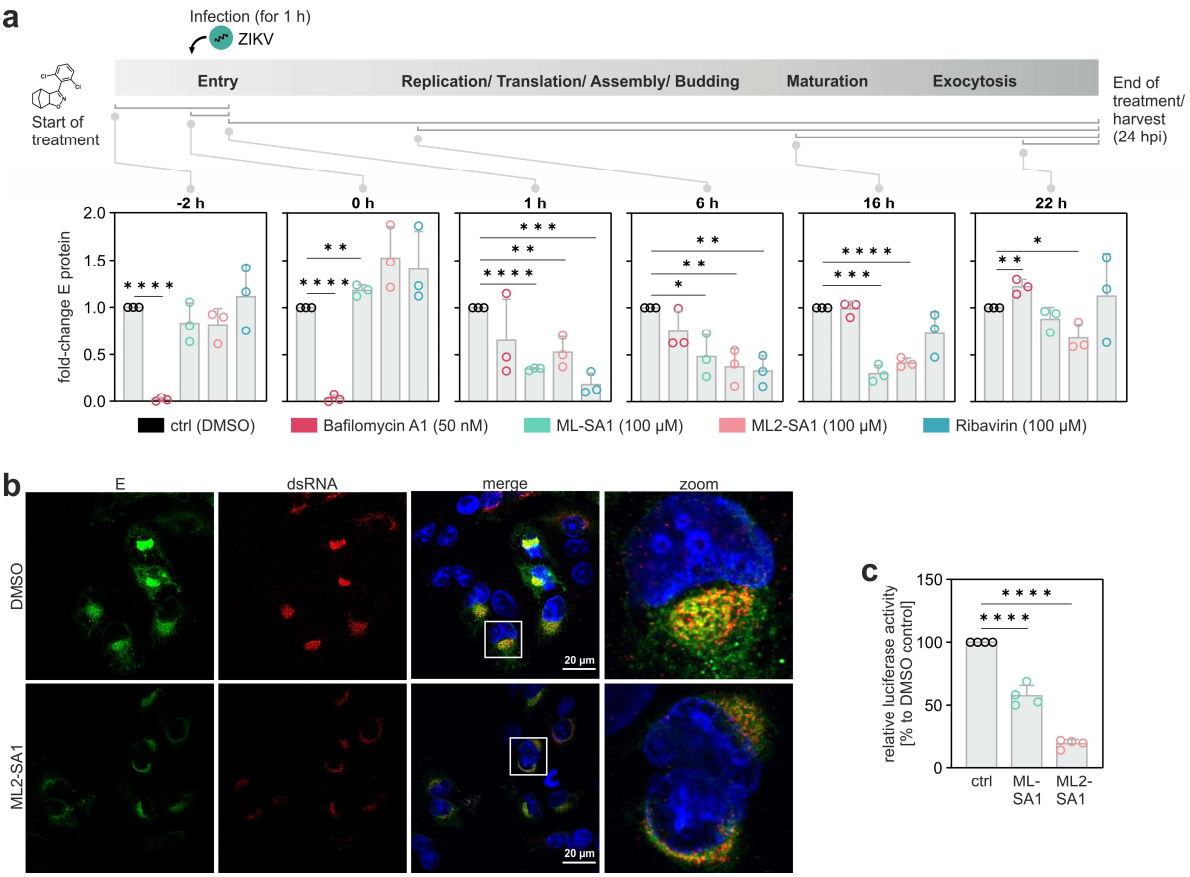

Figure 5: TRPML2 agonist treatment affects late stages of the ZIKV life cycle. (a) A549 cells were infected with ZIKV Uganda isolate (976 Uganda) for one hour (MOI = 1), then unbound virus was removed. Treatment with either 50 nM Bafilomycin A1, 100 µM ML-SA1, 100 µM ML2-SA1 or 100 µM Ribavirin was started at the respective time points, i.e. −2h before infection, during infection, as well as 1 h, 6 h, 16 h or 22 h after infection. Gray brackets below the time scale indicate the respective compound incubation period. The resulting relative fold-change of ZIKV E protein was assessed by Western Blotting. Representative Western Blots are shown in Fig. S6a. Results are normalized to the respective DMSO control of each time point and are expressed as mean ± SD from n = 3 biological replicates. **(b)** Representative confocal laser scanning microscopy (cLSM) images of A549 cells treated with 100 µM ML2-SA1 for 2 h before infection. Cells were infected (MOI = 1) with the ZIKV Uganda (976 Uganda) isolate and fixed 24 hpi. Nuclei were stained with DAPI (blue). ZIKV E protein (green) and ZIKV dsRNA (red) were visualized using specific antibodies. Scale bar: 20 µm. **(c)** A549 cells were treated with 100 µM ML-SA1 or 100 µM ML2-SA1 and simultaneously infected with ZIKV *R*Luc reporter virus for 4 h. Compounds were refreshed during each media change. 48 h post infection, luciferase activity was determined. Results are normalized to the DMSO control and are expressed as mean ± SD from $n = 4$ biological replicates. Statistical significance was determined by using an unpaired *t*-test. *$p < 0.05$, **$p < 0.01$, ***$p < 0.001$, ****$p < 0.0001$.

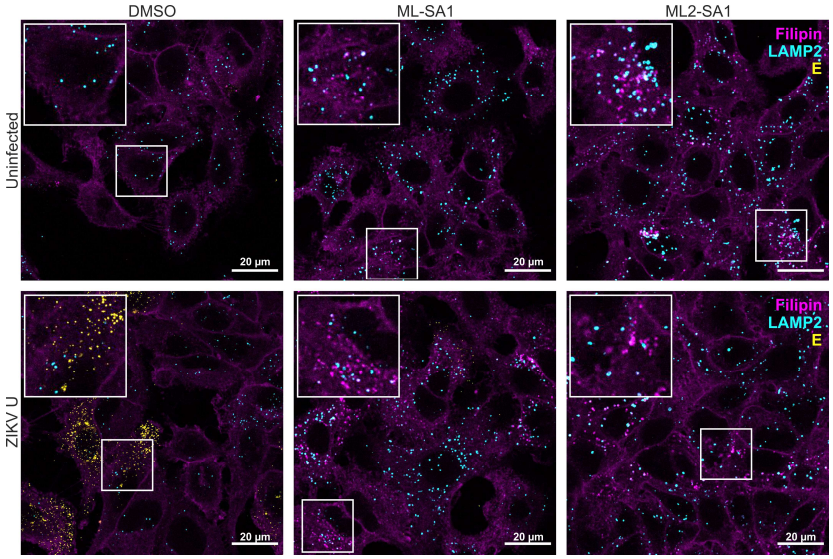

Figure 5: Treatment with ML-SA1 or ML2-SA1 leads to cholesterol accumulation in uninfected and infected cells. Representative confocal laser scanning microscopy images of A549 cells treated with 100 µM ML-SA1 or 100 µM ML2-SA1 for 2 h before infection. Cells were infected (MOI = 1) with the ZIKV Uganda (976 Uganda) isolate and fixed 24 hpi. Intracellular cholesterol and oxysterols were stained using Filipin (magenta). ZIKV E protein (yellow) and the lysosomal marker LAMP2 (cyan) were visualized using specific antibodies. Scale bar: 20 µm.

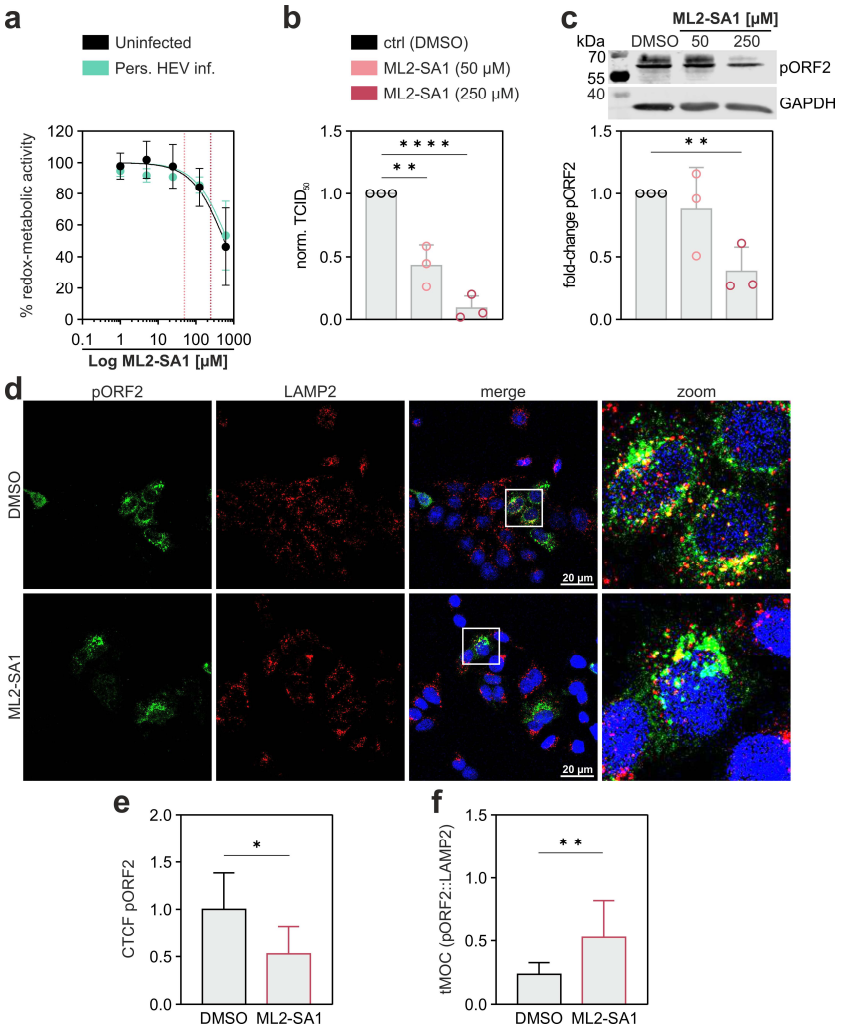

Figure 6: ML2-SA1 reduces intracellular HEV capsid protein by increasing lysosomal degradation and decreases the number of released virions. **(a)** Cell viability of uninfected (black) and persistently HEV-infected (green) A549 cells after treatment with 1 µM to 625 µM ML2-SA1 for 24 h assessed with the PrestoBlue® assay. Values are expressed as % of intact cells normalized to the experimental control. ML2-SA1-concentrations of 50 µM (light pink) and 250 µM (dark pink) are indicated by dotted lines. **(b)** Amount of released infectious HEV particles. **(c)** Relative fold-changes in HEV pORF2 protein of persistently infected A549 cells treated with different concentrations of ML2-SA1. Cells were harvested 24 h post-treatment followed by Western blotting to detect viral pORF2. Data are normalized to the respective DMSO control and are expressed as mean ± SD from $n = 3$ biological replicates, a representative blot is shown above. Statistical significance was determined by using an unpaired *t*-test. $*p < 0.05$, $**p < 0.01$, $***p < 0.001$, $****p < 0.0001$. **(d)** Representative confocal laser scanning microscopy (cLSM) images of persistently HEV-infected A549 cells treated with 250 µM ML2-SA1. Cells were fixed 24 h post treatment. Nuclei were stained with DAPI (blue), HEV pORF2 (green) and LAMP2 (red) were visualized using specific antibodies. Scale bar: 20 µm. **(e)** Normalized signal intensities of HEV pORF2 in micrographs depicted in (d) calculated by corrected total cell fluorescence (CTCF). Data are expressed as mean ± coefficient of variation (CV). **(f)** Absolute degree of co-localization between pORF2 and LAMP2 in (d) determined by calculation of thresholded Mender's overlap coefficient (tMOC); 0 represents no colocalization; 1 represent a complete overlap of signals. Data are expressed as mean ± CV.

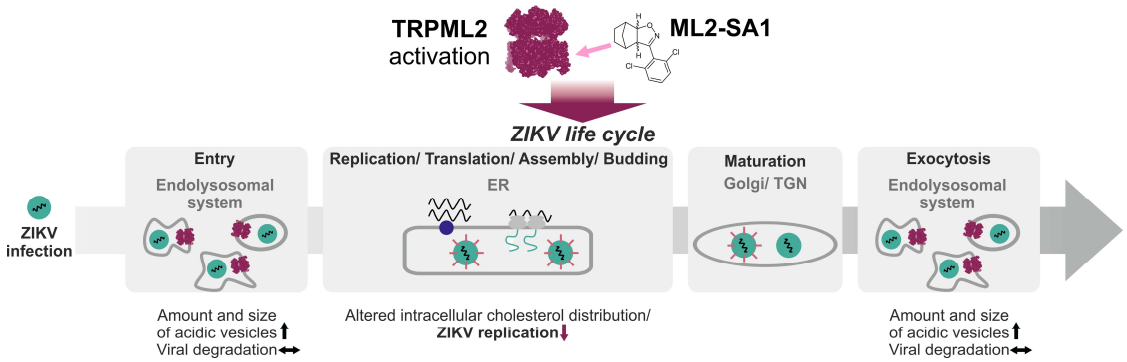

Figure 7: Specific TRPML2 agonist affects multiple stages of the ZIKV life cycle. Treatment with the TRPML2 agonist ML2-SA1 caused increased acidification of the endolysosomal system, however, enhanced lysosomal degradation of ZIKV was not the basis of the antiviral effect of TRPML2 activation. Instead, ML2-SA1 impaired ZIKV replication, presumably by an altered intracellular cholesterol distribution.